Environmental Toxicology and Pharmacology 121 (2026) 104915

Contents lists available at ScienceDirect

Environmental Toxicology and Pharmacology

journal homepage: www.elsevier.com/locate/etap

On-site ALI versus submerged culture: Chemical and toxicological investigation of brake wear sub-micrometric particles

Bozhena Tsyupa [a,d], Chiara Emma Campiglio [b], Elena Carrara [c], Marta Ripamonti [c], Alessandro Mancini [d], Andrea Bonfanti [d], Micol Introna [e], Ana Teresa Juarez-Facio [e], Karine Elihn [e], Manuela Teresa Raimondi [a], Andrea Remuzzi [b,*]

[a] Department of Chemistry, Materials and Chemical Engineering "G. Natta", Politecnico di Milano, Italy
[b] Department of Management, Information and Production Engineering, University of, Bergamo, Italy
[c] Department of Biomedical Engineering, Istituto di Ricerche Farmacologiche Mario Negri IRCCS, Bergamo, Italy
[d] Materials Engineering & Laboratories, GCF Research & Development, Brembo NV, Stezzano, Italy
[e] Department of Environmental Science, Stockholm University, Stockholm, Sweden

ARTICLE INFO

Keywords:
Non-exhaust
Brake wear emissions
In vitro toxicity
Air liquid interface
Dynamometric bench

ABSTRACT

Poor air quality is a significant risk to human health and the environment, with a direct correlation to respiratory diseases and premature death. Ultra fine particles (UFPs) in the atmosphere are particularly hazardous. This study evaluates the toxicological response of epithelial cells (A549) and macrophages (dTHP-1) to particulate matter (PM) emissions from car brake wear, under both submerged and Air-Liquid Interface (ALI) conditions. Toxicity was assessed using cell viability (Resazurin assay) and cytokine assays. Emissions were collected using a dynamometric bench simulating driving and braking conditions. Under ALI, freshly emitted particles were directly deposited onto cells, while in submerged conditions, particles were collected on filters and then deposited onto cells. M1a and M1b materials were tested, both materials are falling into category of ECE R90 Low Metallic pads. M1a showed slight toxicity under ALI and significant immune response in submerged conditions, while M1b showed no toxicity in either condition.

1. Introduction

Air pollution remains one of the most pressing global environmental challenges, posing severe risks to both human health and ecosystems. Among airborne pollutants, fine particulate matter (PM) is of particular concern due to its strong association with respiratory and cardiovascular diseases and increased premature mortality (Pope, Dockery, 2006, Thorpe, Harrison, 2008, WHO, 2013, European Environment Agency (EEA) (EEA) 2020). Road transport is a major contributor to particulate emissions, accounting for approximately 10 % of total PM_{10} and 11 % of $PM_{2.5}$ emissions in Europe (European Environment Agency (EEA) (EEA) 2020). However, limited data exist regarding its contribution to sub-micrometric and ultrafine particles (UFPs), which are thought to exert even greater toxicological effects. Road traffic emissions can be broadly categorized into exhaust (combustion-related) and non-exhaust emissions (NEE), the latter arising from brake, tire, and road wear, as well as resuspended dust. Within NEE, brake wear alone is estimated to contribute roughly 55 % of PM_{10} and 25 % of $PM_{2.5}$ in Europe (Daellenbach et al., 2020, European Environment Agency (EEA) (EEA) 2020). Yet, the contribution of brake wear to the generation of finer particle fractions remains poorly characterized (Mathissen et al., 2011, Barosova et al., 2018, Stojanovic et al., 2022).

Braking systems are essential safety components that convert kinetic energy into heat through friction between the brake disc and pads. This process inevitably leads to material abrasion, producing airborne brake wear particles (BWPs) of diverse sizes and compositions (Thorpe, Harrison, 2008, Kukutschová et al. 2009, Denier van der Gon et al., 2013, Olofsson, 2013, Amato et al., 2014, Grigoratos, Martini, 2015). The quantity and nature of these emissions depend on multiple factors, including braking intensity, material composition, wear mechanisms, and environmental conditions (Mancini et al., 2021, 2023). BWPs are typically rich in iron, oxygen, and carbon, which together constitute approximately 90 % of their total mass, with trace amounts of various other metals and compounds. While larger particles rapidly settle, finer

* Corresponding author.
E-mail addresses: bozhena.tsyupa@polimi.it, bozhena.tsyupa@brembo.com (B. Tsyupa), andrea.remuzzi@unibg.it (A. Remuzzi).

https://doi.org/10.1016/j.etap.2025.104915
Received 31 July 2025; Received in revised form 6 November 2025; Accepted 16 December 2025
Available online 17 December 2025

particles remain suspended, contributing to ambient particulate matter pollution.

With the rapid electrification of road transport, the relative importance of NEE is expected to increase, eventually surpassing exhaust emissions as the dominant source of airborne particulates. Consequently, understanding the chemical composition and toxicological effects of brake-related NEE has become a key research focus (Kumah et al., 2023, Costagliola et al., 2024). However, most studies to date have focused on micrometric fractions (PM_{10} and $PM_{2.5}$), leaving sub-micrometric and ultrafine fractions (<1 μm) largely unexplored (Yingyue, Kumar, 2025). This represents a significant knowledge gap, as smaller particles exhibit higher surface area-to-volume ratios, enhanced reactivity, and increased potential to penetrate biological barriers (Geiser, Kreyling, 2010, Hong, Jee, 2020). Particles in the nanometric (<100 nm) and sub-micrometric (100 nm–1 μm) size ranges can reach the alveolar region of the lungs (Portugal et al., 2024), where they may induce oxidative stress, inflammation, and cytotoxicity, contributing to diseases such as asthma, COPD, and cardiovascular dysfunction (Kwon et al., 2020; Vaze et al., 2024). Sub-micrometric particles generated during the braking process are complex mixtures of inorganic and organic components, which have implications in oxidative stress, inflammation, and cytotoxicity in respiratory cells. It is reasonable to assume that overall similar chemical composition and toxicity effects can be ascribed to nanometric and submicrometric particles. However, specific studies on these dimensional fractions are substantially missing in literature. Thus, this study aims at bridging this identified knowledge gap. *In vitro* models using various human lung cell lines, including A549, BEAS-2B, and Calu-3 cells, are increasingly employed to assess toxicity response to airborne emissions, in both submerged and air-liquid interface (ALI) exposure models (Upadhyay, Palmberg, 2018, Srikanth Vallabani, Gruzieva, 2023). Submerged exposure is a conventional method where cells are exposed to particles suspended in a liquid medium. This condition allows straightforward assessment of cytotoxicity assays and measurements of oxidative stress and inflammation, but it is very distant from the real-life inhalation exposure to airborne particles (Gualtieri et al., 2005, Gasser et al., 2009, Puisney et al., 2018). ALI models are more physiologically relevant for studying toxicity of inhaled aerosols. In ALI exposure, cells are maintained at the interface of air, allowing direct contact between cells and emissions suspended in form of aerosol. Some studies have shown that exposure to particulate matter under ALI conditions results in higher cytotoxicity, enhanced oxidative stress, and greater inflammatory responses compared to submerged conditions (Bessa et al., 2023).

This study focuses on the physico-chemical characterization and evaluation of toxicological effects of brake wear particles produced during braking events of passenger cars. Using lung epithelial adenocarcinoma cell line (A549) and human acute monocytic leukemia cells (dTHP-1). The research investigates the cellular responses to the brake wear particles under two different exposure conditions: submerged and on-site ALI. The experimental setup involves the generation of brake emissions using a dynamometric bench, which replicates standard driving and braking conditions as defined by the Worldwide Harmonized Light Vehicle Test Procedure for Brakes (WLTP-Brake) cycle (Mathissen et al., 2018). Studies on the toxicity of airborne particles using ALI exposure systems are scarce, and none have been conducted by directly connecting dynamometric bench to a mobile ALI system. Our investigation addresses this gap by utilizing a mobile ALI exposure system, called ELLIE (ELectrostatic air-Liquid Interface Exposure system) (Juárez-Facio et al., 2024). For the aims of this work, we hypothesize that the mobile ALI system enables the assessment of the cytotoxic and proinflammatory effects of two brake materials at low doses, in comparison to the conventional submerged exposure approach. Additionally, emissions derived from the two brake materials were collected to facilitate a comprehensive evaluation at higher doses under submerged exposure conditions. Emissions are chemically characterized to assess compositional differences and identify triggers of the toxicological effects. The study utilized Scanning Electron Microscopy (SEM) coupled with Energy Dispersive X-ray Spectroscopy (EDS), Raman Spectroscopy and X-ray Diffraction (XRD) techniques to characterize the morphology and chemical composition of the emitted sub-micrometric particles. For toxicity testing, cell metabolic activity was evaluated using the Resazurin assay, and cytokine release was analyzed.

2. Experimental

2.1. Materials

Two friction pairs (*i.e.*, the coupling of a brake rotor and a brake pad pair), labeled M1a and M1b, both composed by the coupling of a grey cast-iron disc and ECE R90 Low Metallic pads were studied. Despite their similarities in chemical composition, these materials exhibit distinct behaviors in terms of braking performance, which may influence their toxicological impact. These pairs were selected because they represent standard materials widely used in the EU automotive fleet. All selected materials are already available on the market.

2.2. Brake wear generation and collection

Non exhaust brake emissions were collected on aluminum substrates during tests conducted under laboratory-controlled conditions. The brake components were tested using a variable inertia dynamometric bench specifically designed to determine brake emission factors (Mathissen et al., 2018). A more detailed description of the bench can be found in the literature (Perricone et al., 2015), and a schematic of the test platform is provided in the Fig. 1. It should be noted that the dynamometric bench does not fully comply with the most recent design guidelines provided in the UN GTR No.24 (n.d.)(United Nations Global Technical Regulation) on Laboratory Measurement of Brake Emissions for Light-Duty Vehicles, since the experimental campaign was conducted prior to the its final publication (Fig. 2).

In particular, main differences in comparison to the GTR design were: i) the pipe diameter (< 190 mm); ii) a vertical sampling tunnel direction (while horizontal direction is suggested); and iii) the outlet 90° bend radius, which is lower than two times the pipe diameter. Particulates are sampled during the execution of the WLTP-Brake cycle, which consists of a standardized sequence of 303 brake events divided into ten different sectors. Emissions are collected over several repetitions of the WLTP-Brake cycle to gather a sufficient amount of material for chemical and toxicological characterization. The braking corner used for all tests consists of: i) a four-piston fixed aluminum caliper with a piston diameter of 44 mm; ii) a vented brake disc with a diameter of 342 mm and a thickness of 32 mm; and iii) a pair of brake pads with a surface area of 89.1 cm^2. All tests are performed at a fixed inertia of 72.67 kg m^2. During the test, a controlled particle-free air flow of 400 m^3 /h entered the brake enclosure to meet temperature targets, as suggested by recent guidelines from the Particle Measurement Programme (PMP) Informal Working Group (Particle Measurement Programme (PMP) (PMP) (2020)). The air flow was filtered through a HEPA-H13 filter, ensuring an average filtration efficiency over 99.95 %. The entire testing platform was maintained in a controlled environment at 23°C and 50 % relative humidity. Brake emissions were collected by isokinetic sampling using a probe equipped with sharp-edged nozzles for high-efficiency sampling. The sampling line ends in a Dekati Gravimetric Impactor (DGI), which separates different dimensional fractions of the generated particulates. DGI is a high-flow cascade impactor, which collects particles in five size fractions below 2.5 μm. The instrument operates at a flow rate of 95 L/min, with a cyclone providing the first size cut at 2.5 μm. Aluminum substrates were used for the upper four stages, while a 47 mm Teflon filter (pore diameter of 3 μm) serves as the filter at the bottom collection stage. The size ranges for particles collected on stages S1, S2, S3, and S4 are as follows: S1: D50 < 150 nm, S2: D50 < 450 nm,

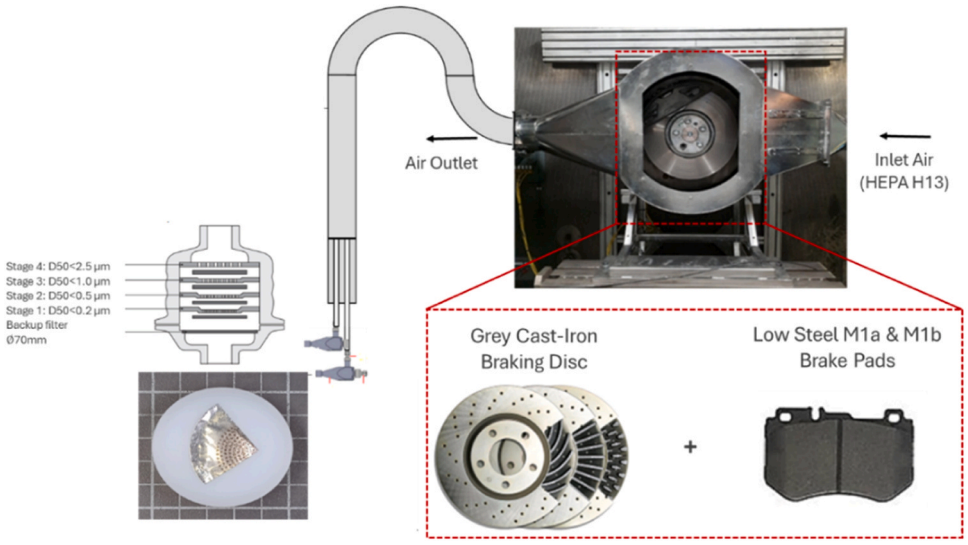

Fig. 1. Schematic image of the experimental setup for collection of the emissions. The image illustrates the airflow path through the system, where HEPA H13 filtered air enters the inlet, passes through the main test chamber and exits through the air outlet simulating a controlled environment for the collection of the brake wear emissions. On the left, schematic of a 4-stage cascade impactor, which separates aerosol particles based on aerodynamic diameter. The image on the left shows a section of the filter from Stage 2, visibly with particles on its surface after an experimental run.

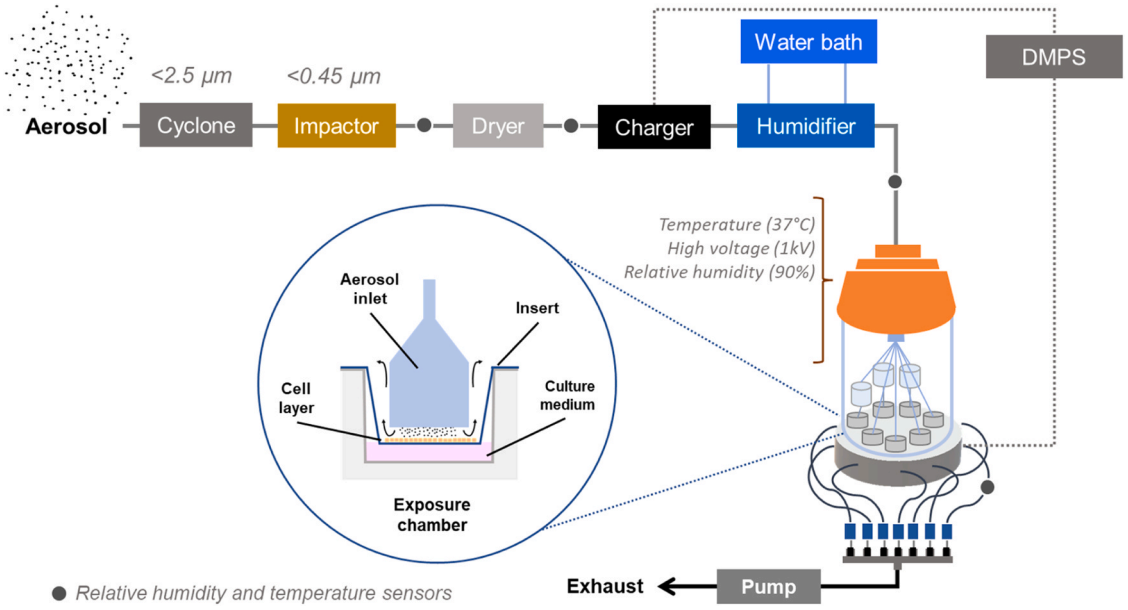

Fig. 2. Schematic overview of the set-up of the ELLIE system. Aerosols from dynamometric bench are directed via a cyclone and an impactor, where particles are size-selected. The aerosol is dried, then charged and humified before being directed to the seven chambers in the exposure module. Two of the exposure chambers are supplied with filters. Particle deposition is augmented by applying an electrostatic force between the aerosol inlet and the electrode below the exposure chamber (Reprinted with authorization from Juárez-Facio et al. 2024).

S3: D50 < 900 nm, S4: D50 < 2.2 µm. The material collected on S2 was used for physicochemical characterization and toxicity tests in submerged mode.

2.3. Sample preparation

Different sample preparation methods were used depending on the specific physico-chemical analysis being conducted. For SEM/EDS and XRD analysis, particulates were first stripped from the filters via sonication in isopropyl alcohol, followed by recovery through centrifugation. Specifically, the collection filters were placed in a 5 mL glass vial containing isopropyl alcohol and sonicated at 35 kHz for 5 min. After sonication, the filter was removed, and the resulting suspension was centrifuged at 3000 rpm for 3 min. Most of the alcohol was then removed with a micropipette, and the remaining solvent was allowed to evaporate overnight at room temperature under mild vacuum conditions (20 mbar), resulting in free powders of brake emissions. For SEM/EDS characterization, this powder was manually applied to an aluminum stub covered with carbon tape for electron microscopy, using a fine-tip, non-magnetic metallic spatula to create a compact layer suitable for electron microscopy. A portion of the prepared powder was also directly used for XRD analysis, while for Raman Spectroscopy analysis, emissions collected on Stage 2 were analyzed right on the collection substrate, without any further manipulation.

2.4. Brake wear particle characterization

2.4.1. Sem/Eds

Scanning Electron Microscopy (SEM) was utilized to qualitatively evaluate the morphology and granulometry of the collected emissions. Initially, SEM was employed to quickly verify the consistency of the dimensional distributions relative to the sampling before proceeding with chemical analysis. Subsequently, the elemental composition of the samples was determined using Energy Dispersive X-Ray Spectroscopy (EDS). The EDS analysis was performed with a Zeiss EVO MA10 electron microscope, equipped with an Oxford Instrument INCA X-act silicon-drift detector (SDD) featuring a 10 mm^2 active area. During EDS spectrum acquisition, backscattered electrons were used to enhance phase contrast and optimize the interaction volume between the particles and the electron beam. The SEM measurements were conducted under specific conditions, with an accelerating voltage (V) of 20 kV and a beam current (I) of 300 pA. For chemical analysis, measurements were taken on five distinct areas, each measuring 400×300 μm. Results of elemental composition were then obtained as average over these five independent observations and standard deviation over the five measures was used as variability index. The chemical composition results were averaged to produce final elemental concentration values, accompanied by a variability index (standard deviation based on five independent observations). Each emission spectrum was acquired within the 0.1–20 keV energy range over 540 s, with the detector dead time maintained below 10 %. The spectra were collected at the optimal working distance for the SEM configuration, which is 8.5 ± 0.1 mm from the electron gun to the sample surface. The sensitivity in this experimental set-up was estimed of 0.01 % in weight for all the identified elements.

SEM images of the morphology and granulometry of the collected emissions are acquired using a Tescan Amber X instrument in Ultra High-Resolution mode. Secondary electron detection was employed to emphasize the morphology of the particles. Prior to imaging, samples were covered with a thin gold coating layer of 5 nm using a Leica EM ACE600 sputter coater. The imaging conditions were set with an acceleration voltage of 5 keV and a beam current of 300 pA.

2.4.2. XRD

The crystalline fraction of the emission powders was analyzed using X-Ray Diffraction (XRD). The analysis was performed using a Rigaku SmartLab diffractometer, which features a rotating anode and a X-Rays source made by a Copper target, thus having characteristic $K_{\alpha 1Cu}$ radiation of 0.154 nm. Measurements were carried out in Bragg-Brentano, *i.e.* para-focusing geometry. The XRD patterns were acquired over an angular range of 5–90° in 2θ, with a step size of 0.02°. For the DGI Stage 2 collected emissions, the scan speed was set at 0.1°/min, resulting in a measurement time of approximately 15 h. The diffracted beam was collected using a standard scintillator detector positioned after a dedicated monochromator at the specific aim of maximizing the resolution of the diffracted beam. To minimize any potential preferential orientation effects, the samples were rotated at 10 rpm during the measurements. Considering the limited amount of available samples as well as the low crystallinity of the composing phases, the estimed detection limit for the experimental set-up described above was expected to be approximatively around 1 % in weight; therefore, it was not possible to identify crystalline phases eventually present in concentrations below this. Phase identification was conducted using the PDF4 + 2023 crystallographic database (ICDD).

2.4.3. Raman spectroscopy

Raman Spectroscopy was employed to further assess the phase composition of the collected emissions, specifically the compounds present in the collected emissions. Raman analysis was conducted using a Horiba LabRAM HR spectrometer, equipped with a 473 nm solid-state laser source. The laser power was nominally set to 25 mW, as higher power levels were found to damage the samples, causing burned micro-areas, while lower power levels did not generated a sufficient signal. All spectra were acquired using a 10X microscope objective, which provide the optimal magnification to maximize the signal-to-noise ratio. Higher magnification objectives were found to be less effective due to the non-homogeneous dispersion of the material and the smaller analysis area compared to the 10X objective. The acquisition range was set between 50 and 2000 cm^{-1} , and to enhance the collected signal, a high-intensity grating of 600 gr/mm was used. A higher grating, such as 1200 gr/mm, was avoided due to the strong fluorescence effect it produced. For each spectrum, twenty accumulations each of five seconds were combined along the entire frequency range.

2.5. Mobile ALI system

A mobile ALI system, known as ELLIE, enables *in vitro* toxicological studies of aerosols directly sampled from the dynamometric bench (Juarez 2024.). Aerosol (1.5 L/min) was drawn through stainless steel tubing from the dynamometric bench into the ALI system. Before entering the ALI system, the aerosol passed through a gas dryer (MD-110–12S-4, Perma Pure, Lakewood, USA) to remove humidity. The aerosol was then charged using a customized Ni-63 neutralizer and subsequently humidified to over 90 % with a humidifier (MH-110–12S-4; Perma Pure, Lakewood, USA) connected to a water bath. The humidified aerosol was distributed to the seven exposure chambers of the ALI system. Inserts containing A549 cells at the ALI condition were placed in each chamber, with medium in the basal compartment. Five chambers were exposed to the full aerosol (gases and particles), while in two chambers, the aerosol was filtered (Headline filters, In-line filter, GradeDIF-LN40), in order to expose cells only to the filtered air, serving as an internal control. Each chamber had a controlled airflow of 214 mL/min, regulated by individual critical orifices. To ensure efficient particle deposition on the cells, an alternating electrostatic field (switching polarity every 4 s) of ±1 kV was applied between the aerosol inlet and the metal plate beneath the exposure chambers. The system maintained a constant temperature of 37°C and relative humidity above 90 % throughout the exposure period. In this configuration, M1a and M1b materials and the same dynamometric bench were used, as for the submerged condition. Before entering the ALI system, emissions from the dynamometric bench passed a $PM_{2.5}$ cyclone, followed by an impactor with a D50 cut-off corresponding to 450 nm. This configuration ensures that only particles with diameters below 450 nm entered the ALI system. Due to ALI system limitations, it was not possible to complete the entire WLTP-Brake Cycle with the on-site ALI system, which last 8 h. Trip 10, the most energetic segment of the WLTP-Brake cycle was selected, which last 2 h. This on-site ALI approach allows for direct particle deposition onto A549 cells, preserving the physico-chemical properties of the emissions without further manipulation. To evaluate the quantity of material deposited onto the cells, a Condensation Particle Counter TSI-3775 (CPC) was used. The CPC was positioned both at the inlet and outlet of the ALI system, and the difference in particle numbers between these two points allows to quantify the mass (μg/cm^2) of particles deposited onto the cells. The CPC operates at the same airflow rate as the ALI system, set at 1.5 L/min.

2.6. Cell Culture

For submerged experiments A549 cells (alveolar epithelial cells derived from human lung adenocarcinoma) were cultured in Kaighn's Modification of Ham's F-12 medium, supplemented with 1 % penicillin/streptomycin (P/S), and 10 % fetal bovine serum (FBS). Cells were kept in a humidified atmosphere at 37 °C, 5 % CO_2, and seeded in 96-well plates, 24 h prior to exposure to PM, at a density of 10000 cells/well.

The cell density was chosen based on existing protocols in the literature, which considered cell size, allowing for a cell confluency of approximately 80 % at the time of exposure.

THP-1 (human acute monocytic leukemia cells) were cultured in RPMI-1640 medium supplemented with 10 % FBS, 1 % P/S, and 1 % L-glutamine. Cells were grown in a humidified atmosphere at 37 °C, 5 % CO_2. 48 h prior to exposure to PM, THP-1 cells were seeded in 96-well plates at a density of 55000 cells/well. Complete medium was supplemented with 50 ng/mL phorbol 12-myristate 13-acetate (PMA) to induce THP-1 differentiation into macrophages (dTHP-1). The number of cells seeded per well was selected to obtain approximately 80 % confluency at the time of exposure.

For ALI experiments, A549 cells were seeded on 6-well Transwell insert, 24 h prior to exposure to PM, at a density of 170000 cells/insert and cultured using the same medium reported above.

2.6.1. Particle removal from filters

According to the amount of particle collected, a fraction of aluminum foil was cut, weighed, and sterilized under a biological hood by exposure to UV light for 30 min. The filter piece was transferred into a sterile glass vial, and sterile MilliQ® H_2O supplemented with 1 % P/S and 2.5 μg/mL of Amphotericin B was added. The suspension was vortexed for 10 min ensuring that the filter remained soaked, and subsequently subjected to sonication for 20 min. The filter was removed, dried completely, and re-weighed. Difference in filter weight was calculated to determine the particle concentration considering the actual volume of suspension in the vial.

2.6.2. Exposure of brake wear particles

2.6.2.1. Submerged culture. 24 h (A549) or 48 h (differentiated THP-1, dTHP-1) post seeding, cells in 96-well plates were gently washed once with pre-warmed Dulbecco's Phosphate-Buffered Saline (PBS), and exposed for 24 h to 100 μL of particle suspensions. Starting from the suspension of extracted particles, a stock solution at 100 μg/mL was prepared in complete medium supplemented with 2.5 μg/mL of Amphotericin B. The same medium was used to further dilute particles at 75, 50, and 10 μg/mL. A concentration of 0 μg/mL was used as negative control. Additional controls, prepared in complete medium supplemented with Amphotericin B, included: LPS at 1 μg/mL (Lipopolysaccharide used as positive control for cytokines release), and extraction from a blank filter (Bk). Each treatment/control was performed in triplicates and each experiment repeated three times (n = 3).

2.6.2.2. Air-liquid interface system. The cells were transported in inserts under ALI conditions for approximately 5 min from the laboratory to the testing facility. Prior to placing the inserts into the mobile ALI system, 3.3 mL of A549 complete medium supplemented with 25 mM HEPES was added to the basal side of cell inserts. During the experiment, no medium was applied to the apical side of the cells to maintain the ALI condition. The cells were exposed for 2 h to brake wear aerosols and filtered air. Filtered air exposed samples were considered as negative control. During the exposure no CO_2 was added, since in a previous study on the validation of the ELLIE system for use in outdoor environments found no effect of not adding CO_2 during exposure, as HEPES helped maintain the pH of the medium between 7.2 and 7.4 (Juárez-Facio et al., 2024). After the exposure, the inserts were transferred to a new 6-wells plate containing 2 mL of fresh complete medium supplemented with 25 mM HEPES on the basal side and transported back to the laboratory. They were then incubated for 24 h.

After incubation, cell viability was measured using the Resazurin assay, and the culture medium was collected, centrifuged at 1500 rpm for 10 min, and stored at −80°C until cytokine levels were determined. Each brake material was tested in at least three independent experiments (n = 3).

2.6.3. Biological endpoints

2.6.3.1. Cell viability assay. After supernatant collection for cytokines analysis, cells were subjected to Resazurin assay to measure the metabolic activity. Resazurin stock solution (0.1 mg/mL in PBS) was diluted to 10 % in complete culture medium and then added to cells and subsequently incubated for 2 h. For the blank, the same solution was in parallel added to three empty wells. Fluorescence was measured using a Tecan plate reader (TECAN Infinite M200 PRO, excitation 530 nm, emission 590 nm). Cell viability was calculated by subtracting the mean value of blanks to each measurement and then expressed as a ratio of the mean of the negative control (i.e., medium with 0 μg/mL particles for submerged test, and filtered samples for ALI), arbitrarily set at 100 %.

2.6.3.2. Cytokines assay. To assess the inflammatory effect of brake wear emissions in A549 and dTHP-1, a multiplex immunoassay was performed targeting 4 different inflammatory cytokines. For both submerged and ALI experiments, after 24 h of cell exposure to particle and controls, supernatants from the basal side for ALI were collected. Supernatants were centrifuged at 1500 rpm for 10 min, and stored at −80 °C. To assess the inflammatory effect of the collected particles, cytokines released were measured using Luminex-based assays and commercially available ELISA (MILLIPLEX plate) kit for the analysis of the supernatant cytokine concentrations. The antibody precoated plates allowed for simultaneous quantification of the following cytokines: Interleukin 1 beta (IL-1β), Interleukin 6 (IL-6), Interleukin 8 (IL-8) and Tumor necrosis factor alpha (TNF-α). Cytokines analysis from three independent experiments were carried out at the same time within a single plate to reduce variability, following manufacturer's instructions. dTHP-1 supernatants were diluted 1:2 in Assay Buffer for the analysis of IL-1β, IL-6, and TNFα, that were assayed in a unique plate suitable for the detection of the selected analytes. IL-8 was analyzed separately, diluting samples of a factor of 200. A549 supernatants were directly tested for the release of IL-1β, IL-6, IL-8 and TNFα without any dilutions.

2.6.3.3. Statistical analysis. Results are expressed as means ± standard deviation. Statistical analysis was performed using GraphPad Prism software (GraphPad Software Inc., version 9). Significant differences between two sets of data were determined by One-way ANOVA followed by Dunnett's correction for multiple comparisons and a value of $p < 0.05$ was considered statistically significant (*$p < 0.05$, **$p < 0.01$, ***$p < 0.001$, ****$p < 0.0001$).

3. Results

3.1. Morphological and Elemental Characterization (SEM-EDS)

SEM analysis in Fig. 3 provides images of particulates generated by both M1a and M1b friction pairs. A visual inspection of the SEM images qualitatively shows that the size distribution of the collected particulates aligns well with the expected range.

Table 1 outlines the elemental concentrations of the brake wear emissions collected from DGI - Stage 2. The collected emissions share similar chemical profiles, with their composition being predominantly iron, oxygen and carbon, which together account for approximately 90 % of the collected mass. The remaining fraction consists of various secondary and trace elements. Carbon, a key indicator of brake material wear, is commonly present in several forms, such as organic resins used as binders, elemental carbon (graphite and coke) as solid lubricants, and inorganic compounds like carbides and carbonates, which function as abrasives or fillers. A smaller, though not negligible amount of carbon may also originate from brake disc wear, as brake rotors are composed of cast-iron, which contains up to 4 wt% carbon. Iron can be traced to the wear of both the brake disc and the friction material, as it is the primary component of the brake disc and is also present in significant quantities

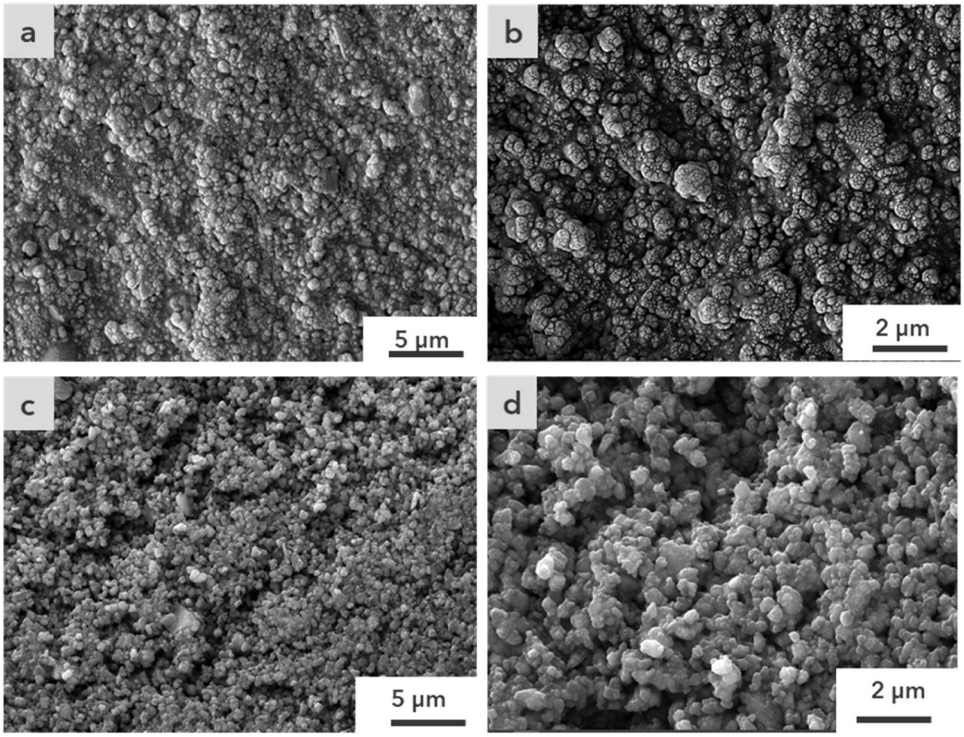

Fig. 3. SEM images of particulates generated by M1a and M1b friction pairs and sampled on S2: 400 <D50 < 450 nm, DGI stage. **a)** M1a at 20x and **b)** M1a at 50x magnifications; **c)** M1b at 20x and **d)** M1b at 50x magnifications.

Table 1
Summary of elemental composition of investigated emissions from DGI-S2. Elemental concentrations are average results over five independent observations, expressed as weight percentage and reported together with the corresponding standard deviations.

M1a – S2			M1b – S2		
Element	**wt%**	**SD**	**Element**	**wt%**	**SD**
Fe	42.7	1.7	**Fe**	44.4	2.4
O	25.5	1.3	**O**	25.4	2.0
C	15.7	1.1	**C**	16.8	3.6
Zn	7.3	0.8	**Sn**	2.8	0.1
Sn	2.6	< 0.1	**Zn**	2.5	0.1
Mg	1.8	0.1	**Mg**	1.9	< 0.1
Si	1.5	0.1	**Al**	1.7	0.1
S	1.1	< 0.1	**Si**	1.5	0.1
Cr	0.5	< 0.1	**S**	1.5	< 0.1
Al	0.4	< 0.1	**Cr**	0.4	< 0.1
Mn	0.3	< 0.1	**Mn**	0.4	< 0.1
K	0.3	< 0.1	**K**	0.3	< 0.1
Cu	0.2	0.1	**Cu**	0.3	< 0.1
Ti	0.08	< 0.1	**P**	0.04	< 0.1
Others	*balance*	-	**Others**	*balance*	-

in friction composites, typically as structural reinforcement. Oxygen can result from tribo-oxidation at the interface of the friction pair, involving metallic species, or from the abrasion of inorganic oxides, silicates, and carbonates commonly used in friction materials as abrasives or fillers. The secondary and trace elements mainly stem from the wear of friction lining composites, with only minor contributions from alloying elements or impurities in cast iron, such as Si, Cr, Mn, and Cu.

The zinc content is three times higher in M1a than in M1b, while tin shows up in both samples in about the same amount. For all other elements (Mg, Ti, Si, Cu, S, Cr, Al, Mn, K, P), the concentrations are consistently low in both M1a and M1b, with no significant differences. Slight differences in the amount of these elements are likely due to distinct tribological mechanisms from the specific friction pairs, influencing the contributions of materials worn from the rotor and pads. These results are consistent with the expected composition of low-metallic brake pads (Grigoratos, Martini, 2015; Mancini et al., 2021).

3.2. X-ray Diffraction and Raman Spectroscopy Analysis

X-ray diffraction patterns of M1a and M1b are presented in Fig. 4 A. For both the samples, crystalline phases are dominated by iron oxides (Fe_3O_4 and Fe_2O_3). M1a pattern suggests a larger amount of iron oxide phases compared to M1b. The peaks are broad and not very intense, which signals low crystallinity or small particle size. The presence of elemental iron (Fe) and carbon (C) suggests contributions from direct abrasion of the brake disc (iron) and possibly friction materials (carbon). The M1a sample shows stronger peaks for metallic iron and carbon compared to M1b. Raman spectra of friction pairs M1a and M1b are presented in Fig. 4B. One of the key features are the characteristic D and G bands, at 1355 cm^{-1} and 1570 cm^{-1} , respectively. These peaks are commonly associated with carbon-based materials. The G band corresponds to the $E_{2\,g}$ mode of graphite, indicating the presence of graphitic or sp^2-bonded carbon atoms. The D band is associated with disordered carbon or the presence of defects within the carbon structure, such as those found in amorphous carbon or other non-crystalline forms. The bands suggest the presence of carbon-based materials from organic binders, graphite, or other carbon-containing components of the brake pads lining material. The M1a sample exhibits significantly stronger intensity for both the D and G bands compared to the M1b sample. This suggests that the carbon in M1a is more crystalline (graphitic) in nature. Instead, the relatively weaker signals in the M1b sample imply a more amorphous carbon structure with less graphitic content. Notably, these findings are in good agreement with observations from XRD analysis.

The low-wavenumber peaks at 215 cm^{-1} and 280 cm^{-1} are typically associated with iron oxides. They are more pronounced in the M1a spectrum, suggesting a higher content of crystalline iron oxide phases in this sample compared to M1b. The oxides are probably related to the wear of the brake disc or other metallic components in the friction pair.

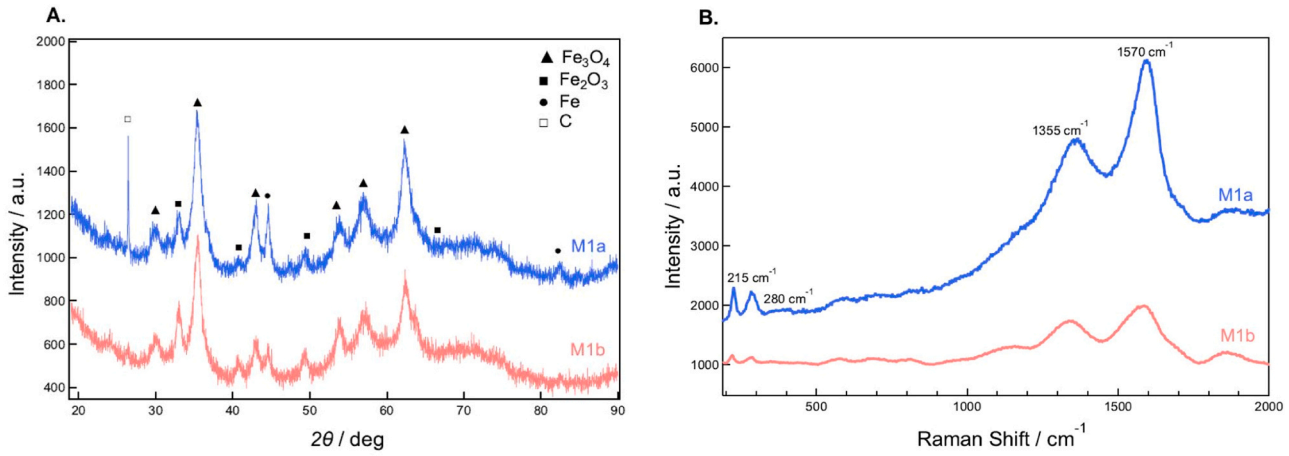

Fig. 4. (A.) X-ray diffraction (XRD) patterns of particles generated by friction pairs M1a (blue) and M1b (red). The peaks correspond to various crystalline phases, including Fe_3O_4 (magnetite, ▲), Fe_2O_3 (hematite, ■), elemental iron (Fe, ●) and carbon (C, □). (B.) Raman spectra of sub-micrometric particles generated from friction pairs M1a (blue) and M1b (red). The spectra reveal characteristic peaks at 215 cm^{-1} and 280 cm^{-1} , which are attributed to metal oxides, and prominent D (1355 cm^{-1}) and G (1570 cm^{-1}) bands, indicating carbonaceous materials.

3.3. Biological endpoints: in vitro exposure to brake wear particles

3.3.1. Submerged exposure

The cell viability results for submerged exposures to brake wear emissions collected in a controlled laboratory environment are presented in Fig. 5. No significant decrease in cell viability was observed in A549 cells for any of the tested concentrations (10, 50, and 75 μg/mL) or friction pair (M1a and M1b). Conversely, a slight reduction in viability was detected in dTHP-1 cells upon exposure to material M1a at the highest concentration.

Interestingly, both A549 and dTHP-1 cells exhibited an increase in viability compared to the control when exposed to material M1b. However, this increase in metabolic activity cannot be conclusively attributed to a biological response without considering a potential interference of material M1b with the assay used.

Overall, dTHP-1 cells appeared to be more sensitive to particle exposure, as evidenced by a significant reduction in viability following treatment with M1a. This decrease was comparable to the difference observed between the negative control and the blank filter sample. Therefore, it cannot be definitively concluded that the reduction in viability at the highest M1a concentration is solely due to the test material; the volume of water used for particle extraction may also have influence in the observed cytotoxicity.

The release of cytokines IL-8, IL-6, TNFα, and IL-1β were measured in the dTHP-1 model using three concentrations of brake wear particles (10, 50, and 75 μg/mL), as shown in Fig. 6. No statistically significant differences were observed for material M1b (Fig. 6B). In contrast, material M1a induced a significant increase in IL-8, IL-6, and IL-1β release at the highest concentration, with levels comparable to or even exceeding those of the LPS positive control (Fig. 6A). These results suggested an inflammatory response of dTHP-1 after M1a particle exposure.

3.3.2. ALI exposure

A549 cells were exposed to brake wear emissions using the ALI system. During the ALI sampling, different amounts of brake wear emissions were deposited onto the cells for the M1a and M1b formulations. Specifically, 0.009 μg/cm^2 were deposited onto the cells for M1a, while 0.04 μg/cm^2 were deposited for M1b. The biological effects observed were limited and not significant, likely due to the low amount of material deposited during the exposure period. Cell viability results following ALI exposure to brake wear particles are presented in Fig. 7 A.

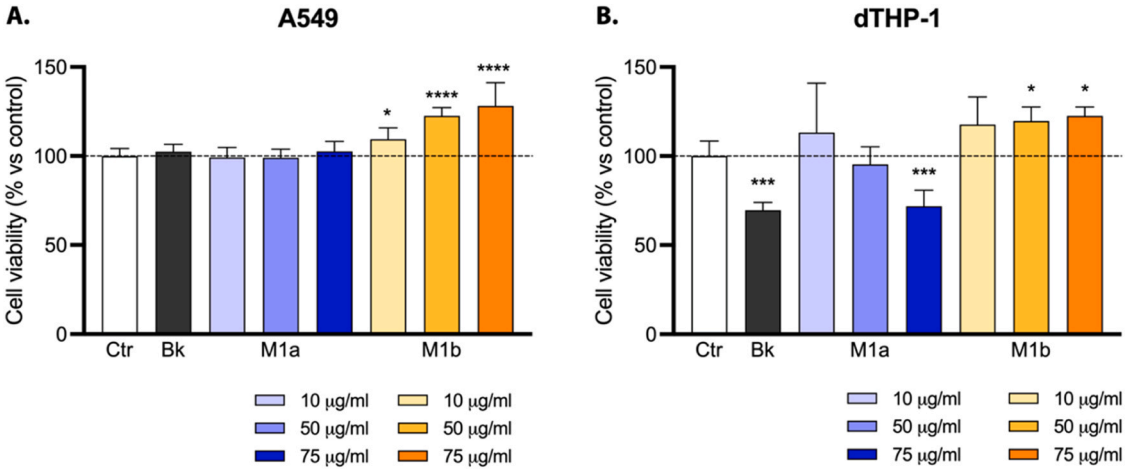

Fig. 5. Cell viability (resazurin assay) of (A) A549 and (B) dTHP-1 following 24 h exposure to brake wear emissions collected in laboratory environment. Two materials were tested M1a and M1b. For each experiment, results were normalized on the mean of the control sample. Data are reported as mean ± SD of data obtained from three independent experiments (n = 3). Differences were established using a one-way ANOVA comparing each sample to the control, followed by Dunnett's correction for multiple comparisons. * $p \leq 0.05$, ** $p \leq 0.01$, *** $p \leq 0.001$, **** $p \leq 0.0001$. Bk, Blank filter. Dashed line, 100 %.

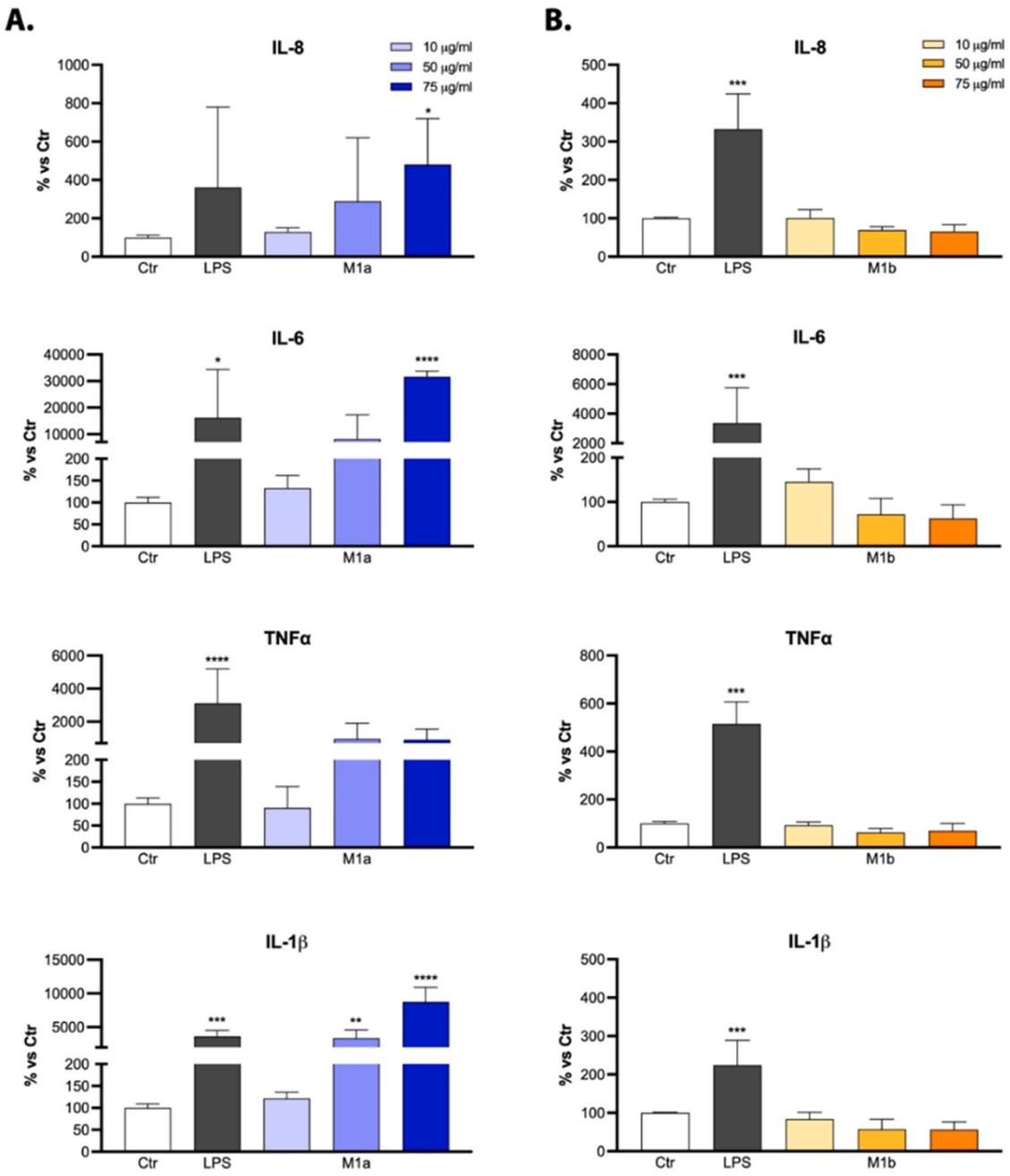

Fig. 6. Cytokines production from dTHP-1 following 24 h exposure to: (A) M1a emission, (B) M1b emission. Results were normalized on the mean of the control sample of each experiment. Data are reported as mean ± SD of data obtained from three independent experiments (n = 3). Differences were established using a one-way ANOVA comparing each sample to the control, followed by Dunnett's correction for multiple comparisons. * $p \leq 0.05$, ** $p \leq 0.01$, *** $p \leq 0.001$, **** $p \leq 0.0001$.

M1a friction pair caused a slight reduction in cell viability compared to control filtered samples. Consistent with the results observed under submerged exposure conditions, M1b friction pair induced a slight increase in A549 cell viability. This effect may not be solely due to the material's stimulation of cellular metabolic activity, as interference from particulate matter with the assay cannot be ruled out. No significant differences were detected in cytokine levels for any of the tested materials, as shown in Fig. 7B. IL-6, IL-1β, and TNF-α values were below the detection limit and are therefore not reported. The reduction in IL-8 levels observed following exposure to material M1b appears statistically significant compared to the control sample.

4. Discussion

The primary aim of this study was to evaluate the physicochemical properties and toxicological effects of airborne particulate matter emitted by brakes wear, specifically particles in the range of D50 < 450 nm, using an innovative mobile ALI exposure system. This novel setup, which directly connects to the dynamometric bench, allows for the real-time collection and exposure of freshly emitted particles without further manipulation, thus preserving the aerosol properties for more accurate toxicological assessment. Our findings demonstrate that the use of the ALI system offers a valuable tool for studying non-exhaust emissions, particularly from brakes wear.

Chemical analysis of the brake wear emissions of the inorganic part,

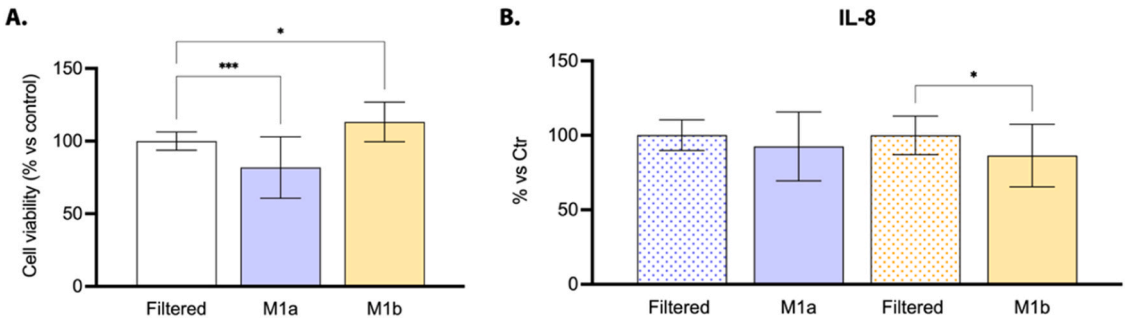

Fig. 7. (A) Cell viability and (B) IL-8 cytokine production of A549 following 2 h exposure collected by using ALI system. Data are reported as mean ± SD of data obtained from three independent experiments (n = 3). Differences were established using a one-way ANOVA comparing each sample to the control, followed by Dunnett's correction for multiple comparisons. * $p \leq 0.05$, ** $p \leq 0.01$, *** $p \leq 0.001$, **** $p \leq 0.0001$.

revealed that both M1a and M1b formulations were predominantly composed of iron oxides, metallic iron and carbon, which is consistent with the elemental composition of typical brake wear dust. Notably, the M1a formulation contained significantly higher amounts of zinc (7.3 wt %) compared to M1b (2.8 wt%), a difference that is likely to play a crucial role in the observed toxicological effects. Zinc, a known heavy metal, has been associated with adverse biological effects, including oxidative stress, inflammation, and cytotoxicity. Previous studies have reported that high concentrations of zinc can exacerbate toxicological responses in various cell lines, including A549 cells, which were used in this study for ALI exposure experiments (Lu et al., 2015, Park et al., 2007, Prieditis, Adamson, 2002, Uski et al., 2014). Aside from the previously mentioned difference in Zn based compounds content, we lack information on the organic compounds, making it unclear if there could be any other distinctions between the two formulations.

The toxicity assessments conducted in ALI conditions showed a slight decrease in cell viability for M1a. These results are consistent with previous studies that have demonstrated cytotoxic responses when cells are exposed to Zn or ZnO fine particles. For example, nano-ZnO particles have been found to induce significant cytotoxicity, as evidenced by a reduction in cell viability and increased levels of lactate dehydrogenase (LDH), a marker of membrane damage (Lu et al., 2015, He et al., 2017; Ng et al., 2017). However, no significant cytokine change was observed for M1a or M1b under ALI exposure, which could be attributed to the specific conditions under which the exposure was conducted, such as the low doses or the direct interaction between the aerosol and the cell layer.

In submerged conditions, the toxicity responses differed slightly from those at ALI conditions. The M1a formulation caused a modest reduction in cell viability in dTHP-1 cells, suggesting that immune cells may be more sensitive to brakes wear particulates than epithelial cells. This observation aligns with findings from other studies that highlight the increased sensitivity of immune cells to particulate exposure, as these cells are often at the forefront of the body's response to environmental pollutants (Gray et al., 2015, Park et al., 2024). Additionally, M1a exposure led to a significant increase in the release of pro-inflammatory cytokines, including IL-8, IL-6, and IL-1β, at the highest concentrations. This inflammatory response was comparable to or even exceeded that of the LPS-positive control, suggesting that the M1a particles induced a modest inflammatory reaction in dTHP-1 cells. These results are consistent with previous research demonstrating that particulate matter, especially that containing metals like zinc, can provoke inflammatory responses in immune cells (Lanone et al., 2009). Zinc has been shown to induce the generation of reactive oxygen species (ROS), which can lead to oxidative stress and inflammation, both of which are implicated in the pathogenesis of various respiratory and cardiovascular diseases (Wallenborn et al., 2009). Moreover, previous studies have identified zinc as a key player in the toxicity of ambient particulate matter, where it was found to contribute to the overall toxicity of fine particulate matter by promoting cell death and inflammatory responses in both *in vitro* and *in vivo* models (Adamson et al., 2000, Riley et al., 2003). Research on the toxicity of airborne particles using ALI exposure systems remains limited, with no prior studies directly linking a dynamometric bench to a mobile ALI system. The use of this ALI system allows for a more realistic exposure scenario, as particulate matter is delivered to the cells in its native state, without manipulation or resuspension, closely mimicking real-world conditions. Instantaneous doses in the ALI setup are intended to reflect potential urban exposure scenarios. The benefits of this approach arise from the combination of these factors: direct delivery of unaltered particles, more representative exposure conditions, and the ability to better simulate real-life inhalation events.

5. Limitations

The results from this study provide valuable insights into the toxicological impacts of brake wear emissions, however there are some limitations that should be considered. One of the limitations is the low concentration of brake wear particles, resulting in a relatively small amount of collected particles. For submerged conditions, emissions were collected throughout the entire WLTP cycle, whereas for ALI sampling, emissions were only collected during Trip 10 of the WLTP cycle. This was due to the ELLIE system's limitation, which supports sampling durations of less than 2 h. However, Trip 10 of the WLTP cycle corresponds to the most energetic trip, thus the one generating the higher amount of particulate. Additionally, emissions for submerged conditions required extra processing and extraction steps. The doses tested for submerged and ALI conditions also differed due to the varying sampling times. The second limitation is the lack of assessment of the organic components of the emissions. While the study focused on the inorganic fraction, the organic compounds in brakes wear, such as polycyclic aromatic hydrocarbons (PAHs), may also play a significant role in the overall toxicity of the emissions. Moreover, the gaseous components of the aerosol were not considered in this study, even though volatile organic compounds (VOCs) and other gases present in brake wear emissions have been shown to contribute to toxicity (Gminski et al., 2010). However, since the resins used in both M1a and M1b formulations are identical and the temperatures reached during the test are the same, the observed differences in toxicity are unlikely to be attributed to the organic part of the emissions. Future studies should incorporate the evaluation of both the organic and gaseous components to provide a more comprehensive understanding of the toxicological effects of brake wear emissions. Additional limitation is that we were only able to test two formulations, M1a and M1b, because these tests are quite expensive. Another limitation arises from the differences between submerged and ALI conditions. In general, co-cultures in ALI exposures represent an interesting model that better mimics an exposure by inhalation, however, as this study is part of a European project, the choice of monocultures in the ALI experiments was done to compare the different results between the other collaborators.

6. Conclusions

The study aimed to evaluate the toxicological effects of airborne particulate matter emitted by brake wear using an innovative mobile ALI exposure system. Notably, the ALI system was used for the first time in direct connection to a dynamometric bench suitably designed for brake emission testing. Chemical analysis showed that both M1a and M1b formulations were mainly composed of iron oxides, metallic iron, carbon and a wide set of secondary elements, with M1a containing higher amounts of Zn. This difference in Zn based compounds content likely plays a crucial role in the observed toxicological effects. Indeed, in submerged conditions, M1a caused a modest reduction in cell viability in dTHP-1 cells and a significant increase in pro-inflammatory cytokines, suggesting that immune cells may be more sensitive to brake wear particulates than epithelial cells. Toxicity assessments under ALI conditions showed a slight decrease in cell viability for M1a. Therefore, findings from this work suggest that the mode of exposure and composition of brakes emissions are both determining factors for the toxicological outcomes. These results underscore the need for further investigation to understand the mechanisms behind the toxicity of brake wear particles. The study highlights the importance of considering both inorganic and organic components in future research to provide a comprehensive understanding of the toxicological effects of brake wear emissions. Nevertheless, reported findings demonstrated how ALI systems can be used as additional valuable tool for assessing non-exhaust emissions from brake wear.

CRediT authorship contribution statement

Andrea Bonfanti: Visualization. **Micol Introna:** Visualization, Formal analysis, Data curation. **Marta Ripamonti:** Visualization, Formal analysis. **Alessandro Mancini:** Writing – review & editing, Visualization, Validation, Supervision, Investigation, Formal analysis, Data curation. **Elena Carrara:** Visualization, Methodology. **Bozhena Tsyupa:** Writing – review & editing, Writing – original draft, Visualization, Validation, Supervision, Methodology, Investigation, Formal analysis, Data curation, Conceptualization. **Chiara Emma Campiglio:** Writing – review & editing, Writing – original draft, Formal analysis, Data curation. **Raimondi Manuela:** Visualization. **Andrea Remuzzi:** Visualization. **Ana Teresa Juarez-Facio:** Writing – review & editing, Visualization, Data curation. **Karine Elihn:** Visualization, Formal analysis.

Declaration of Competing Interest

The authors declare the following financial interests/personal relationships which may be considered as potential competing interests: Bozhena Tsyupa reports financial support was provided by European Union. If there are other authors, they declare that they have no known competing financial interests or personal relationships that could have appeared to influence the work reported in this paper.

Acknowledgments

This research was supported by the European Commision's Horizon 2020 research and innovation programme: nPETS (grant agreement No 954377, https://www.npets-project.eu)

Data availability

Data will be made available on request.

References

Adamson, I.Y., Prieditis, H., Hedgecock, C., Vincent, R., 2000. Zinc is the toxic factor in the lung response to an atmospheric particulate sample. Toxicol. Appl. Pharm. 166 (2), 111–119. https://doi.org/10.1006/taap.2000.8955.

Amato, F., Cassee, F., Denier van der Gon, Hugo A.C., Gehrig, R., Gustafsson, M., Hafner, W., Querol, X., 2014. Urban air quality: The challenge of traffic non-exhaust emissions. J. Hazard. Mater. 275, 3136. https://doi.org/10.1016/j.jhazmat.2014.04.053).

Barosova, H., Chortarea, S., Peikertova, P., Clift, M.J.D., Petri-Fink, A., Kukutschova, J., Rothen-Rutishauser, B., 2018. Biological response of an in vitro human 3D lung cell model exposed to brake wear debris varies based on brake pad formulation. Arch. Toxicol. 92 (7), 2339–2351. https://doi.org/10.1007/s00204-018-2218-8.

Bessa, M.J., Brandão, F., Rosário, F., Moreira, L., Reis, A.T., Valdiglesias, V., Teixeira, J. P., 2023. Assessing the in vitro toxicity of airborne (nano)particles to the human respiratory system: from basic to advanced models. J. Toxicol. Environ. Health Part B 26 (2), 67–96. https://doi.org/10.1080/10937404.2023.2166638.

Costagliola, M.A., et al., 2024. Non-exhaust particulate emissions from road transport vehicles. Energies 17 (16), 4079.

Daellenbach, K.R., Uzu, G., Jiang, J., et al., 2020. Sources of particulate-matter air pollution and its oxidative potential in Europe. Nature 587, 414–419. https://doi.org/10.1038/s41586-020-2902-8.

Denier van der Gon, H., Gerlofs-Nijland, M., Gehrig, R., Gustafsson, M., Janssen, N., Harrison, R., Cassee, F., 2013. The Policy relevance of wear emissions from road transport, now and in the future—an international workshop report and consensus statement. J. Air Waste Manag. Assoc. 63 (2), 136–149. https://doi.org/10.1080/10962247.2012.741055.

European Environment Agency (EEA), Air Quality in Europe – 2020 Report. EEA Report No 10/2020 (2020).

Gasser, M., Riediker, M., Mueller, L., Perrenoud, A., Blank, F., Gehr, P., Rothen-Rutishauser, B., 2009. Toxic effects of brake wear particles on epithelial lung cells in vitro. PMID: 19930544; PMCID: PMC2784745 (Part Fibre Toxicol.. https://doi.org/10.1186/1743-8977-6-30.

Geiser, M., Kreyling, W.G., 2010. Deposition and biokinetics of inhaled nanoparticles. Part Fibre Toxicol. 7, 2. https://doi.org/10.1186/1743-8977-7-2.

Gminski, R., Tang, T., Mersch-Sundermann, V., 2010. Cytotoxicity and genotoxicity in human lung epithelial A549 cells caused by airborne volatile organic compounds emitted from pine wood and oriented strand boards. Toxicol. Lett. 196 (1), 33–41. https://doi.org/10.1016/j.toxlet.2010.03.015.

Gray, D.L., Wallace, L.A., Brinkman, M.C., Buehler, S.S., La Londe, C., 2015. Respiratory and cardiovascular effects of metals in ambient particulate matter: a critical review. Rev. Environ. Contam. Toxicol. 234, 135–203. https://doi.org/10.1007/978-3-319-10638-0_3.

Grigoratos, T., Martini, G., 2015. Brake wear particle emissions: a review. Environ. Sci. Pollut. Res 22, 2491–2504. https://doi.org/10.1007/s11356-014-3696-8.

Gualtieri, M., Andrioletti, M., Mantecca, P., 2005. Impact of tire debris on in vitro and in vivo systems. Part Fibre Toxicol. 2 (1). https://doi.org/10.1186/1743-8977-2-1.

He, T., Long, J., Li, J., Liu, L., Cao, Y., 2017. Toxicity of ZnO nanoparticles (NPs) to A549 cells and A549 epithelium in vitro: Interactions with dipalmitoyl phosphatidylcholine (DPPC). Environ. Toxicol. Pharm. 56, 233–240. https://doi.org/10.1016/j.etap.2017.10.002.

Hong, G., Jee, Y.K., 2020. Special issue on ultrafine particles: where are they from and how do they affect us? Exp. Mol. Med 52, 309–310. https://doi.org/10.1038/s12276-020-0395-z.

Juárez-Facio, A., Introna, M., Gustavsson, S., Attergren, M., Lindwall, M., Elihn, K., 2024. A mobile air-liquid interface exposure system optimized for outdoor toxicity testing of aerosols. Aerosol Sci. Technol. 59 (2), 214–226. https://doi.org/10.1080/02786826.2024.2426487.

Kukutschová, J., Roubíček, V., Malachová, K., Pavlíčková, Z., Holuša, R., Kubačková, J., Micka, V., MacCrimmon, D., Filip, P., 2009. Wear mechanism in automotive brake materials, wear debris and its potential environmental impact. Wear 267, 807–817. https://doi.org/10.1016/j.wear.2009.01.034.

Kumah, E.A., Fopa, R.D., Harati, S., Boadu, P., Zohoori, F.V., Pak, T., 2023. Human and environmental impacts of nanoparticles: a scoping review of the current literature. BMC Public Health 23, 1059.

Kwon, H.S., Ryu, M.H., Carlsten, C., 2020. Ultrafine particles: unique physicochemical properties relevant to health and disease. Exp. Mol. Med. 52, 318–328.

Lanone, S., Rogerieux, F., Geys, J., et al., 2009. Comparative toxicity of 24 manufactured nanoparticles in human alveolar epithelial and macrophage cell lines. Part Fibre Toxicol. 6, 14. https://doi.org/10.1186/1743-8977-6-14.

Lu, S., Zhang, W., Zhang, R., Liu, P., Wang, Q., Shang, Y., Wu, M., Donaldson, K., Wang, Q., 2015. Comparison of cellular toxicity caused by ambient ultrafine particles and engineered metal oxide nanoparticles. Part Fibre Toxicol. 12, 5. https://doi.org/10.1186/s12989-015-0082-8.

Mancini, A., Tsyupa, B., Pin, S., Bandiera, M., et al., 2021. SAE Technical Paper, 2021-01-1300, Chem. Brake Emiss. Influ. Test. Cycle. https://doi.org/10.4271/2021-01-1300), 2021-01-1300,.

Mathissen, M., Grochowicz, J., Schmidt, C., Vogta, R., Farwick zum Hagena, F.H., et al., 2018. A Novel Real-World Braking Cycle for Studying Brake Wear Particle Emissions. Wear (14–415), 219–226. https://doi.org/10.1016/j.wear.2018.07.020.

Mathissen, M., Scheer, V., Vogt, R., Benter, T., 2011. Investigation on the potential generation of ultrafine particles from the tire–road interface. Atmos. Environ. 45 (34), 6172–6179. https://doi.org/10.1016/j.atmosenv.2011.08.032.

Ng, C.T., Yong, L.Q., Hande, M.P., Ong, C.N., Yu, L.E., Bay, B.H., Baeg, G.H., 2017. Zinc oxide nanoparticles exhibit cytotoxicity and genotoxicity through oxidative stress

responses in human lung fibroblasts and Drosophila melanogaster. Int J. Nanomed. 12, 1621–1637. https://doi.org/10.2147/IJN.S124403.
Olofsson, U., 2013. On the emission of airborne wear particles from disc brakes. Wear 297 (1-2), 819–825.
Park, S., Lee, Y.K., Jung, M., Kim, K.H., Chung, N., Ahn, E.K., Lim, Y., Lee, K.H., 2007. Cellular toxicity of various inhalable metal nanoparticles on human alveolar epithelial cells. Inhal. Toxicol. (1), 59–65. https://doi.org/10.1080/08958370701493282.
Park, M., Park, S., Choi, Y., et al., 2024. The mechanism underlying correlation of particulate matter-induced ferroptosis with inflammasome activation and iron accumulation in macrophages. Cell Death Discov. 10, 144. https://doi.org/10.1038/s41420-024-01874-y.
Particle Measurement Programme (PMP), Informal Working Group, Informal document GRPE_81_12, 81st GRPE, 9-11 June, Agenda Item 7 (2020).
Perricone, Guido, Wahlstrom, J., Olofsson, U., 2015. Towards a Test Stand for Standardized Measurements of the Brake Emissions. Proc. I. Mech. E. Part D J. Aut. Eng. 1–8. https://doi.org/10.1177/0954407015616025.
Pope, C., Dockery, D., 2006. Health effects of fine particulate air pollution: Lines that connect. J. Air Waste Manag. Assoc. 56 (6), 709–742. https://doi.org/10.1080/10473289.2006.10464485.
Portugal, J., Bedia, C., Amato, F., Juárez-Facio, A.T., Stamatiou, R., Lazou, A., Campiglio, C.E., Elihn, K., Piña, B., 2024. Toxicity of airborne nanoparticles: Facts and challenges. Environ. Int 190, 108889. https://doi.org/10.1016/j.envint.2024.108889.
Prieditis, H., Adamson, I.Y., 2002. Comparative pulmonary toxicity of various soluble metals found in urban particulate dusts. Exp. Lung Res 28 (7), 563–576. https://doi.org/10.1080/01902140290096782.
Puisney, C., Oikonomou, E., Nowak, S., Chevillot, A., Casale, S., 2018. Brake wear (nano) particle characterization and toxicity on airway epithelial cells in vitro. Environ. Sci. 5 (4), 1036–1044.
Riley, M.R., Boesewetter, D.E., Kim, A.M., Sirvent, F.P., 2003. Effects of metals Cu, Fe, Ni, V, and Zn on rat lung epithelial cells. Toxicology 190 (3), 171–184. https://doi.org/10.1016/s0300-483x(03)00162-8.
Srikanth Vallabani, N.V., Gruzieva, O., 2023. Toxicity and health effects of ultrafine particles: Towards an understanding of the relative impacts of different transport modes. ISSN 0013-9351 Environ. Res. 231 (Part 2), 116186. https://doi.org/10.1016/j.envres.2023.116186.
Stojanovic, N., Glisovic, J., Abdullah, O.I., Belhocine, A., Grujic, I., 2022. Particle formation due to brake wear, influence on the people health and measures for their reduction: a review. Environ. Sci. Pollut. Res Int 29 (7), 9606–9625. https://doi.org/10.1007/s11356-021-17907-3.
Thorpe, A., Harrison, R., 2008. Sources and properties of non-exhaust particulate matter from road traffic: A review. Sci. Total Environ. 400 (s 1–3). https://doi.org/10.1016/j.scitotenv.2008.06.007).
UN GTR No.24, (n.d.)Laboratory Measurement of Brake Emissions for Light-Duty Vehicles | UNECE.
Upadhyay, S., Palmberg, L., 2018. Air-Liquid Interface: Relevant In Vitro Models for Investigating Air Pollutant-Induced Pulmonary Toxicity. Jul 1 Toxicol. Sci. 164 (1), 21–30. https://doi.org/10.1093/toxsci/kfy053.
Uski, O., Jalava, P.I., Happo, M.S., Torvela, T., Leskinen, J., Mäki-Paakkanen, J., Tissari, J., Sippula, O., Lamberg, H., Jokiniemi, J., Hirvonen, M.R., 2014. Effect of fuel zinc content on toxicological responses of particulate matter from pellet combustion in vitro. Sci. Total Environ. 511, 331–340. https://doi.org/10.1016/j.scitotenv.2014.12.061.
Vaze, N., Calderon, L., Tsiodra, I., Mihalopoulos, N., Serhan, C.N., Levy, B.D., Demokritou, P., 2024. Assessment of the Physicochemical Properties of Ultrafine Particles (UFP) from Vehicular Emissions in a Commercial Parking Garage: Potential Health Implications. Toxics 12 (11), 833.
Wallenborn, J.G., Schladweiler, M.J., Richards, J.H., Kodavanti, U.P., 2009. Differential pulmonary and cardiac effects of pulmonary exposure to a panel of particulate matter-associated metals. Toxicol. Appl. Pharm. 241 (1), 71–80. https://doi.org/10.1016/j.taap.2009.08.003.
WHO, 2013. Review of evidence on health aspects of air pollution – REVIHAAP Project. World Health Organization.
Yingyue, Wei, Kumar, Prashant, 2025. Beyond the tailpipe: Review of non-exhaust airborne nanoparticles from road vehicles. ISSN 2772-9850 EcoEnviron. Health 4 (1), 100130. https://doi.org/10.1016/j.eehl.2024.11.003.